

Prepolarized MRI of Hard Tissues and Solid-State Matter

José M. González^{*,†}, Jose Borreguero^{*,†}, Eduardo Pallás[‡], Juan P. Rigla[†], José M. Algarín[‡], Rubén Bosch[†], Fernando Galve[‡], Daniel Grau-Ruiz[†], Rubén Pellicer[‡], Alfonso Ríos[†], José M. Benlloch[‡], and Joseba Alonso[‡]

**Equally contributing authors*

[†]Tesoro Imaging S.L., 46022 Valencia, Spain

[‡]MRILab, Institute for Molecular Imaging and Instrumentation (i3M), Spanish National Research Council (CSIC) and Universitat Politècnica de València (UPV), 46022 Valencia, Spain

Instituto de Instrumentación para Imagen Molecular, Centro Mixto CSIC—Universitat Politècnica de València, 46022 Valencia, Spain

Abstract—Prepolarized Magnetic Resonance Imaging (PMRI) is a long-established technique conceived to counteract the loss in signal-to-noise ratio (SNR) inherent to low-field MRI systems. When it comes to hard biological tissues and solid-state matter, PMRI is severely restricted by their ultra-short characteristic relaxation times. Here we demonstrate that efficient hard tissue prepolarization is within reach with a special-purpose 0.26 T scanner designed for dental MRI and equipped with suitable high-power electronics. We have characterized the performance of a 0.5 T prepolarizer module which can be switched on and off in just 200 μ s. To that end, we have used resin, dental and bone samples, all with T_1 times in the order of 20 ms at our field strength. The measured SNR enhancement is in good agreement with a simple theoretical model, and small deviations in extreme regimes can be attributed to mechanical vibrations due to the magnetic interaction between the prepolarization and main magnets. Finally, we argue that these results can be applied to clinical dental imaging, opening the door to replacing hazardous X-ray systems with low-field PMRI scanners.

Index Terms—MRI, low field, prepolarization, hard tissues, solid state

I. INTRODUCTION

LOW-FIELD Magnetic Resonance Imaging (LF-MRI) is gaining momentum as an affordable alternative to clinical MRI, the current gold standard in numerous medical imaging applications, but also extremely expensive and often inaccessible [1], [2], [3]. The main cost driver in an MRI scanner is the superconducting magnet required to generate the strong, static magnetic field (B_0) that enables the high quality images typical for clinical MRI. By lowering the field strength, the need for superconducting magnets is removed, resulting in a drastic reduction of the economic and energetic needs. On the other hand, the signal-to-noise ratio (SNR) of the magnetic resonance signals and reconstructed images is also greatly compromised.

Prepolarization is a long-established technique designed to partially compensate for the SNR loss in LF-MRI [4], [5], [6], [7], [8], and could be of special relevance for hard biological tissues where hydrogen content is sparse and signals decay very fast [9], [10]. In Prepolarized MRI (PMRI), the

Boltzmann equilibrium magnetization of the sample is boosted by an intense, not necessarily homogeneous, magnetic pulse of amplitude B_p before the start of the imaging pulse sequence, which is then executed at a lower but highly homogeneous B_0 . For efficient PMRI, the prepolarization pulse must be turned off in a time t_{off} much shorter than the sample T_1 relaxation time over which the extra magnetization is lost. This is easily met for liquids and soft biological tissues, where spin-lattice interactions are averaged out by the molecular tumbling of water, leading to relaxation times above 100 ms [11]. Indeed, PMRI has already demonstrated its potential for *ex vivo* and *in vivo* imaging of soft samples at field strengths ranging from hundreds of milli-tesla to hundreds of micro-tesla [10], [12], [13], [14], [15], [16]. For solid-state matter or hard biological tissues (e.g. dental tissues), which feature short T_1 times, prepolarization is much more challenging: the suppressed proton mobility prevents the averaging-out of dipolar interactions by molecular tumbling of protons in water. This effect is even more pronounced at low field strengths, where the Larmor frequency is closer to proton tumbling frequencies [17]. On the other hand, hard tissue PMRI could be of relevance for dental clinical practice, where hazardous X-ray systems are massively used [18], and for which there is no affordable MRI alternative as of yet [9], [19], [20], [21].

In this paper, we demonstrate prepolarization and imaging of samples with ultra-short T_1 , down to a few tens of milliseconds. After brief introductions to the relevant theoretical framework and experimental equipment in Secs. II and III respectively, we analyze in Sec. IV the signal strength boost for an inorganic solid-state sample as a function of pulse sequence parameters. Besides revealing the effect of prepolarization, this study also shows that the simple model presented in Sec. II adequately describes the observed data, where deviations can be attributed to the effect of sudden mechanical displacements due to the strong interaction between the main and prepolarization magnets during the prepolarization pulse. In Sec. V, we present the first prepolarized magnetic resonance images (of a cattle bone and a human tooth), which show an SNR increase of a factor of 2 with respect to an equivalent acquisition without prepolarization. Finally, in Sec. VI, we discuss the feasibility of extending the presented MRI concept to clinical

JMG and JB have contributed equally to this work.

Corresponding author: J. Alonso (joseba.alonso@i3m.upv.es).

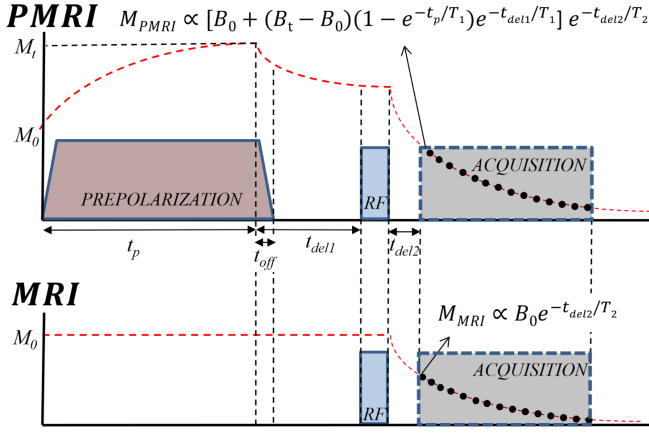


Fig. 1. PMRI (top) and MRI (bottom) pulse sequences used in this work, with analytical expressions for the magnetization at the start of FID acquisition. Their ratio α represents the SNR gain due to prepolarization, as per Eq. (2). M_t and M_0 are the magnetizations in thermal equilibrium with and without prepolarization and are directly proportional to B_t and B_0 respectively.

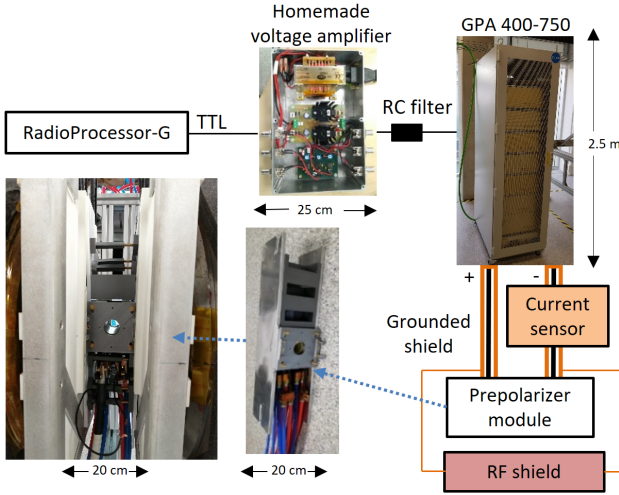


Fig. 2. Scheme of the setup employed for hard tissue PMRI.

applications in the field of dentistry and orthodontics.

II. THEORY

To quantify the effect of the prepolarization on hard tissues, in the remainder of the paper we compare the signals resulting from magnetic pulse sequences based on those in Fig. 1. These sequences are identical except for the fact that the prepolarization pulse has an amplitude B_p in the PMRI sequence and zero in the standard MRI sequence. For an homogeneous sample of characteristic relaxation time T_1 , we define the prepolarization gain α as the ratio between the sample magnetizations during the data acquisitions:

$$\begin{aligned} M_{\text{PMRI}} &\propto \left(B_0 + (B_t - B_0) \left(1 - e^{-t_p/T_1} \right) e^{-t_{\text{del1}}/T_1} \right) e^{-t_{\text{del2}}/T_2}, \\ M_{\text{MRI}} &\propto B_0 e^{-t_{\text{del2}}/T_2}, \end{aligned} \quad (1)$$

so

$$\alpha \equiv \frac{M_{\text{PMRI}}}{M_{\text{MRI}}} = 1 + \frac{B_t - B_0}{B_0} \left(1 - e^{-t_p/T_1} \right) e^{-t_{\text{del1}}/T_1}, \quad (2)$$

where we neglect the duration of RF pulses. Here: $B_t = |\vec{B}_0 + \vec{B}_p|$ is the total field strength during the prepolarization pulse, where the main and prepolarization fields need not be parallel; t_p is the prepolarization pulse length, during which the magnetization asymptotically reaches equilibrium with B_t ; t_{off} is the ramp down time of the prepolarization pulse; $t_{\text{del1}} \geq t_{\text{off}}$ is the time from the moment the prepolarization pulse starts to be switched off until the beginning of the radio-frequency (RF) excitation; t_{del2} is the time between the RF pulse and the start of the data acquisition; and T_2 is the sample-dependent dephasing characteristic time over which the magnetization decoheres. Admittedly, this definition of SNR enhancement tends to overestimate the benefits of PMRI, since the standard MRI sequence could be shortened and its SNR increased by further averaging in the same overall acquisition time. Nevertheless, this is the simplest possible comparison and is typical in the literature (see e.g. [12]).

III. APPARATUS

As a result of the short T_1 timescales typical of solids, hard tissue prepolarization poses a significant engineering challenge to achieve fast enough t_{off} times. Our solution to this follows.

The ‘‘DentMRI - Gen I’’ 0.26 T scanner and prepolarization modules employed for this work (see Fig. 2) are described in detail elsewhere [9], [10]. Essentially, our group has designed, built and characterized a prepolarizer coil whose main parameters of inductance, resistance and efficiency are $L \approx 600 \mu\text{H}$, $R \approx 75 \text{ m}\Omega$ and $\eta \approx 1.9 \text{ mT/A}$. The gap between the planar gradient stacks is $\approx 210 \text{ mm}$, placing a hard boundary on the prepolarizer module size and, consequently, to the maximum achievable coil inductance. Due to geometric limitations and to ease accessibility, we placed the prepolarizer module so that \vec{B}_p is perpendicular to \vec{B}_0 [10]. This reduces the maximum achievable B_t from $|\vec{B}_0| + |\vec{B}_p|$ to $(B_0^2 + B_p^2)^{1/2}$, but has the advantage that the generated Eddy currents and the residual energy in the prepolarization coil barely disturb the longitudinal field \vec{B}_0 (e.g. when B_p falls to 1 mT, the total field deviates from the original B_0 by only $2 \mu\text{T}$).

In order to cope with the short T_1 of hard biological tissues, the high power electronics setup for the prepolarizer module has been substantially upgraded with respect to the system introduced in Ref. [10]. In the current apparatus, a digital output from the RadioProcessor-G board (SpinCore Electronics LLC) is amplified in two stages, first in a homemade variable-gain low-voltage amplifier, and then in a high power (400 A and 750 V) gradient amplifier from International Electric Co. (GPA 400-750). The latter can ramp currents from 0 to $\pm 260 \text{ A}$ in $\approx 200 \mu\text{s}$ in our $\approx 600 \mu\text{H}$ load (see Fig. 3), where we were previously limited to $\approx 35 \text{ ms}$ [10]. Figure 3 also shows a smoother transition corresponding to the case where we low-pass filter the digital output with an RC circuit of characteristic time constant $\approx 350 \mu\text{s}$. We find this convenient to avoid mechanical stress in the module due to the sudden appearance of strong magnetic interactions between the main magnet and the prepolarizer. This reduces the generation of Eddy currents and, thereby, distortions in the acquired signals and image reconstructions due to uncontrolled

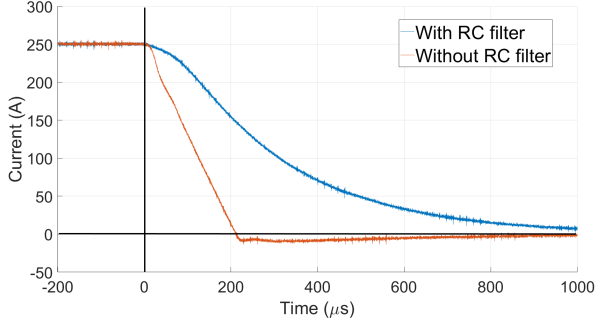


Fig. 3. Falling edge of the prepolarization pulse current from 250 A ($B_p \approx 0.475$ T) with the GPA 400-750, with and without the low-pass RC filter (see text). With the RC filter, the prepolarizer field is 1 mT after ≈ 1.73 ms (not shown), so the deviation of the total field with respect to 0.26 T is just $2 \mu\text{T}$ and the Larmor frequency may be considered stabilized.

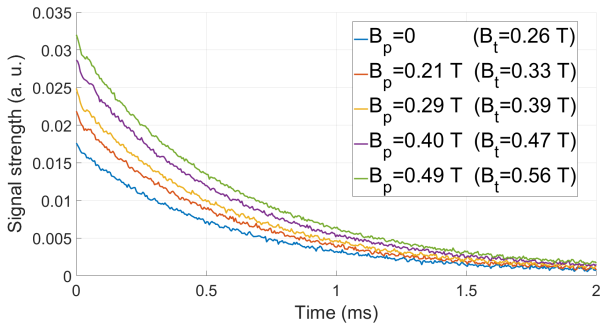


Fig. 4. FIDs after prepolarizing the photopolymer resin sample with pulses of $t_p = 160$ ms and $t_{\text{del1}} = 3$ ms for different B_p values.

magnetic field dynamics. All the measurements below are with the low-pass filter.

IV. SNR ENHANCEMENT

For calibration and first tests we employed a sample made of a photopolymer resin [22], which is highly homogeneous, abundant in hydrogen and features relaxation parameters comparable to the enamel in human teeth. At our B_0 , we have measured $T_1 \approx 23.1$ ms and $T_2 \approx 650 \mu\text{s}$ with Inversion Recovery [23] and CPMG [24], [25] pulse sequences, respectively.

First we check whether the SNR is enhanced by prepolarization as predicted by the model in Eq. (2). To that end, we set $t_p = 160$ ms ($> 7T_1$) in the sequence in Fig. 6 to prepolarize close to the saturation magnetization. Next, a resonant $\pi/2$ RF pulse coherently rotates the magnetization to the transverse plane. Both pulses are separated by a wait time $t_{\text{del1}} = 3$ ms, long enough to avoid Larmor frequency shifts and distortions in the acquired Free Induction Decay (FID) signals due to residual magnetic energy in the prepolarizer. The signal readout starts $t_{\text{del2}} = 100 \mu\text{s}$ after the RF pulse to avoid ring-down from the RF coil. The resulting FID is acquired for $t_{\text{acq}} = 2$ ms with a readout bandwidth $BW = 200$ kHz. This protocol is repeated for four different voltage gains of our home-made amplifier, generating $B_p \approx 0.21, 0.29, 0.40$ and 0.49 T, which correspond to $B_t \approx 0.33, 0.39, 0.47$ and 0.56 T. Figure 4 shows the absolute value of the FIDs for these cases

and for the standard MRI sequence ($B_p = 0$ and $B_t \approx 0.26$ T). For a given value of B_p , we calculate the prepolarization boost $\bar{\alpha}_{B_p}$ as the mean ratio of the PMRI and standard MRI data:

$$\bar{\alpha}_{B_p} = \frac{1}{N_{\text{points}}} \sum_{i=1}^{N_{\text{points}}} \frac{s_{B_p}(t_i)}{s_0(t_i)}, \quad (3)$$

where $N_{\text{points}} = t_{\text{acq}} \cdot BW$, $s_{B_p}(t_i)$ is the signal amplitude measured for the PMRI with prepolarization strength B_p for the time bin (t_i), and $s_0(t_i)$ is the amplitude measured for the standard MRI sequence at t_i . The estimated $\bar{\alpha}_{B_p}$ values are $1.240 \pm 0.005, 1.430 \pm 0.008, 1.705 \pm 0.008$ and 1.964 ± 0.011 for the above prepolarization field strengths, where the given uncertainties indicate the standard error of the mean

$$\sigma_{\bar{\alpha}} = \frac{1}{N_{\text{points}}} \sqrt{\sum_{i=1}^{N_{\text{points}}} \left(\frac{s_{B_p}(t_i)}{s_0(t_i)} - \bar{\alpha}_{B_p} \right)^2}. \quad (4)$$

The corresponding theoretical α values for $T_1 \approx 23.1$ ms can be calculated from Eq. (2): $\alpha \approx 1.24, 1.44, 1.72$ and 1.98 .

The small experimental deviations from the theoretically calculated values could arise from: i) mechanical vibrations due to magnetic forces, ii) induced Eddy currents or iii) off-resonant spin evolution due to a time-dependent Larmor frequency. All three are more pronounced for intense B_p values and short t_{del1} times. To find a working regime free of these effects, we have characterized their influence on the SNR gain with the measurements shown in Fig. 5.

For the plots in Fig. 5 we sweep the prepolarization pulse duration from $t_p = 10$ to 160 ms and t_{del1} from 1 to 4 ms, for the same four B_p values as above. The gain and uncertainty for every data point are estimated according to Eqs. (3) and (4). The solid lines in the figure correspond to calculations employing the model in Eq. (2).

Unsurprisingly, for the weaker prepolarization currents we measure FID curves that follow closely theoretical predictions, even for t_{del1} as short as 1 ms. Deviations are stronger for short wait and prepolarization times. In the extreme case of $B_p \approx 0.49$ T and $t_{\text{del1}} = 1$ ms, the measured data was heavily corrupted and did not follow the typical exponential behavior (i.e. as in the FIDs in Fig. 4). It is unlikely that these issues are due to drifts in the Larmor frequency as the prepolarizer relaxes, since a residual orthogonal field perturbs B_0 very weakly (e.g., for $B_p \approx 0.49$ T and $t_{\text{del1}} = 1$ ms, the Larmor frequency shifts by only 250 Hz). On the other hand, Eddy currents and especially mechanical vibrations can be behind for the aforementioned deviations. In fact, we have observed that these unwanted effects are more prominent if the prepolarizer is not rigidly fixed to the scanner. With the mechanical fixation in place (see Fig. 2), the system performs well away from this extreme regime. Indeed, the plots in Fig. 5 demonstrate that the measured SNR gain is compatible with theoretical predictions for prepolarization pulses longer than 120 ms and $t_{\text{del1}} \geq 2$ ms.

V. HARD TISSUE PMRI

In this section we demonstrate the system's capability for imaging hard biological tissues with PMRI. To that end, we

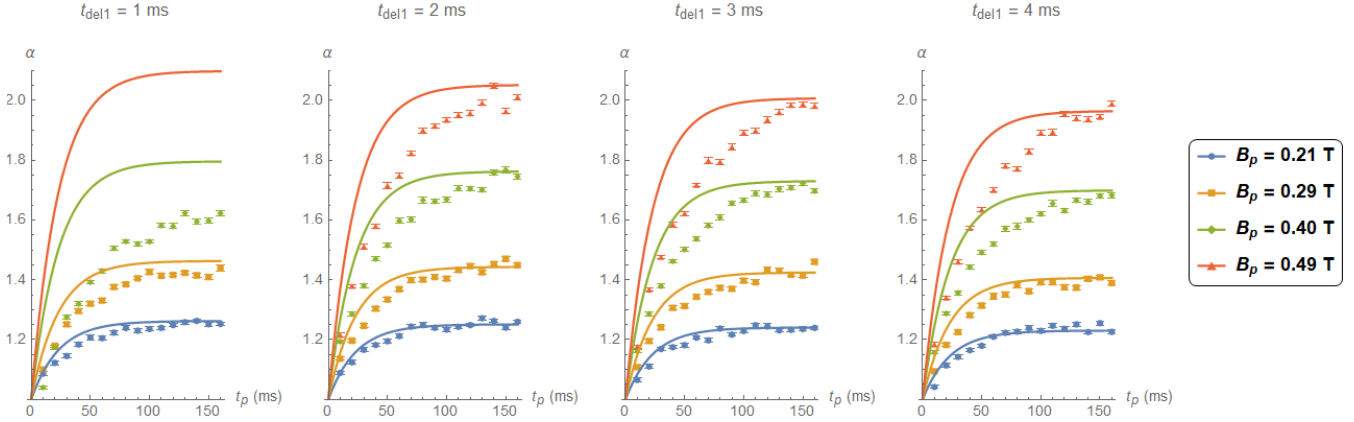


Fig. 5. Comparison between theoretical (continuous lines) and experimental (data points) gain α for different values of t_p , B_p and t_{del1} , using the photopolymer resin sample. The data for $B_p = 0.49$ T is not included because it was heavily corrupted by the sharp magnetic transitions (see text). For a given B_p , the maximum gain decreases with t_{del1} due to T_1 decay after the prepolarization pulse.

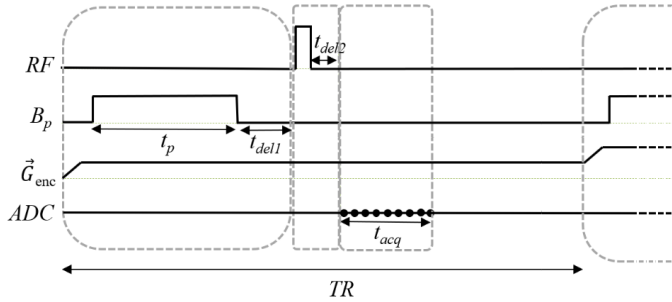


Fig. 6. P-PETRA pulse sequence integrating the PMRI sequence in Fig. 1 with PETRA. P-PETRA is employed for the prepolarized hard tissue images in Figs. 7 and 8. Here, \vec{G}_{enc} is the frequency encoding gradient and the ADC (analog-to-digital converter) acquisition is marked with black points.

employ: i) an adult human molar tooth (Fig. 7(c)) extracted one year before these experiments and dried so that primarily mineralized matter (dentin and enamel) remains; and ii) a piece of cattle rib (Fig. 8(c)) including cortical and spongy bone tissues. We have measured the T_1 times of both samples by Inversion Recovery, and found $T_1 \approx 20.3$ and 19.3 ms for the tooth and bone, respectively. The cattle bone contains both cortical and spongy tissues, so the estimated time is an averaged quantity. The T_1 times of all the employed samples are very similar, so we can determine suitable parameter regimes from the measurements on the photopolymer resin (Fig. 5).

The ultra-short T_2 times typical of hard tissues impose the use of dedicated MRI sequences, such as those in the Zero Echo Time (ZTE) family [26]. These are characterized by radial k -space acquisitions beginning immediately after the RF excitation, to capture as much as possible of the short-lived signal. Ramping the gradient is time consuming, so in ZTE sequences the spatial encoding gradients are switched on before the RF pulse. In this work, we even switch on the frequency encoding gradient before prepolarization [27] to limit mechanical vibrations and the influence of Eddy currents during acquisition. Having the gradient on during resonant excitation imposes the use of hard (short and intense) RF

pulses, leading to spurious signals which could corrupt the data acquisition. To prevent this, we introduce a delay t_{del2} before the readout, resulting in a gap without data at the center of k -space. This can be filled with additional acquisitions [28]. One possibility is to do so in a pointwise fashion, as in PETRA (Pointwise Encoding Time-reduction with Radial Acquisition, [29]). For the following images we employ a PETRA sequence with a prepolarization stage before the RF excitation (P-PETRA, Fig. 6).

In Fig. 7 we show prepolarized images of a human molar tooth obtained following the scheme in Fig. 6. The size of the field of view is set to $21 \times 13 \times 13$ mm³ and the image is reconstructed with Algebraic Reconstruction Techniques (ART, [9], [30], [31]) into $42 \times 26 \times 26$ voxels. The acquisition starts $t_{del1} = 130$ μ s after the RF pulse to avoid the effect of ring-down and lasts $t_{acq} = 700$ μ s, with a bandwidth $BW \approx 30$ kHz. The repetition time is set to $TR = 250$ ms, limited by the maximum duty cycle of the GPA 400-750 at this current regime. We undersample the number of radial lines in k -space by a factor $\times 8$ with respect to the Nyquist criterion, where ART reconstructions are still robust. Every image contains 12 averages for a total scan time of ≈ 29 min. The bottom row of images in Fig. 7(a) corresponds to scans in which a prepolarization pulse is triggered with a current intensity of ≈ 260 A ($B_t \approx 0.56$ T), which lasts $t_p = 90$ ms and where $t_{del1} = 2$ ms. The pulse sequence for the top row of Fig. 7(a) is identical, but the prepolarization pulse is not triggered ($B_p = 0$, $B_t = 0.26$ T). The brightness scale is common to both datasets to highlight the gain in SNR with PMRI. Both images have been denoised using a Block-Matching filter [9], [32]. To quantify the influence of prepolarization, we plot in Fig. 7(b) the same profile along a horizontal line around the upper portion of the images in (a), in the region of the tooth crown. The mean $\alpha = \text{SNR}_{\text{PMRI}}/\text{SNR}_{\text{MRI}}$ (before filtering and averaged over a region of interest of constant bright pixels around the dentin) is ≈ 1.97 , where $\text{SNR}_{\text{PMRI}} = \bar{s}_{\text{PMRI}}/\bar{n}_{\text{PMRI}} \approx 16.46$, and SNR_{MRI} (analogously defined) is ≈ 8.36 . The mean signal and noise values (\bar{s} and \bar{n}) are estimated, respectively, as the mean value and standard deviation of the voxel brightness in the region

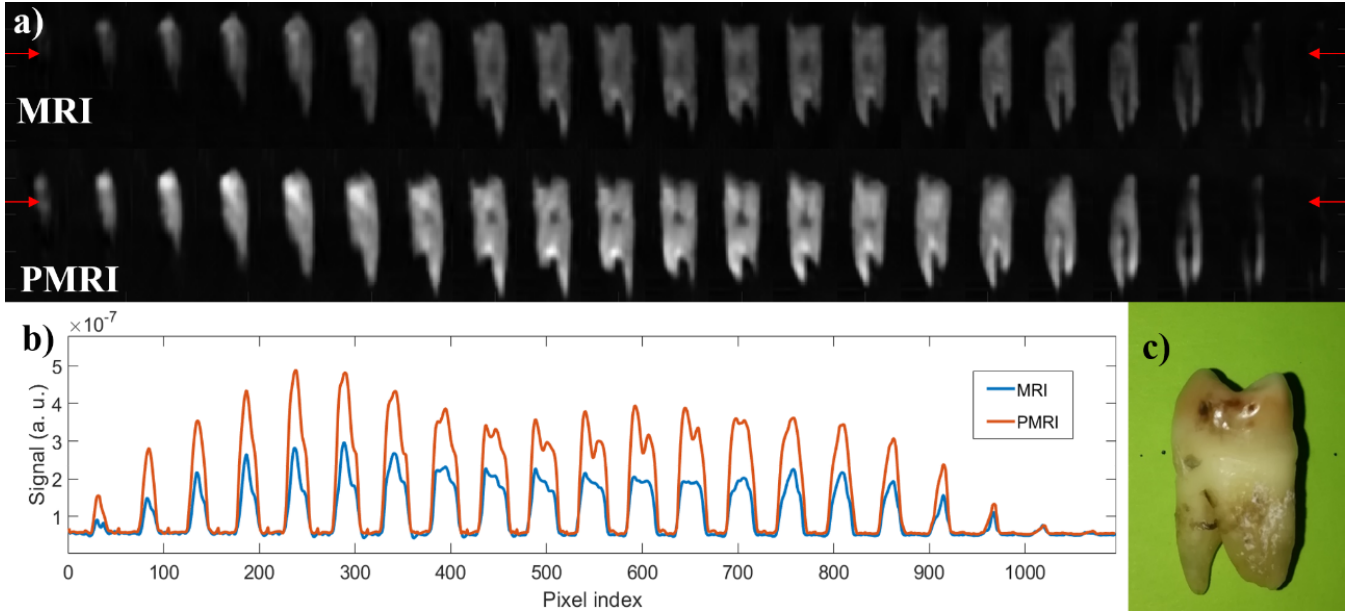


Fig. 7. (a) PETRA (top) and P-PETRA (bottom) images of an *ex-vivo* adult human molar tooth. (b) Signal intensity along the horizontal line defined by the red arrows in (a). The experimentally obtained value for the prepolarization gain is $\alpha \approx 1.97$ (expected value ≈ 2.02 , see text). (c) Photograph of the sample.

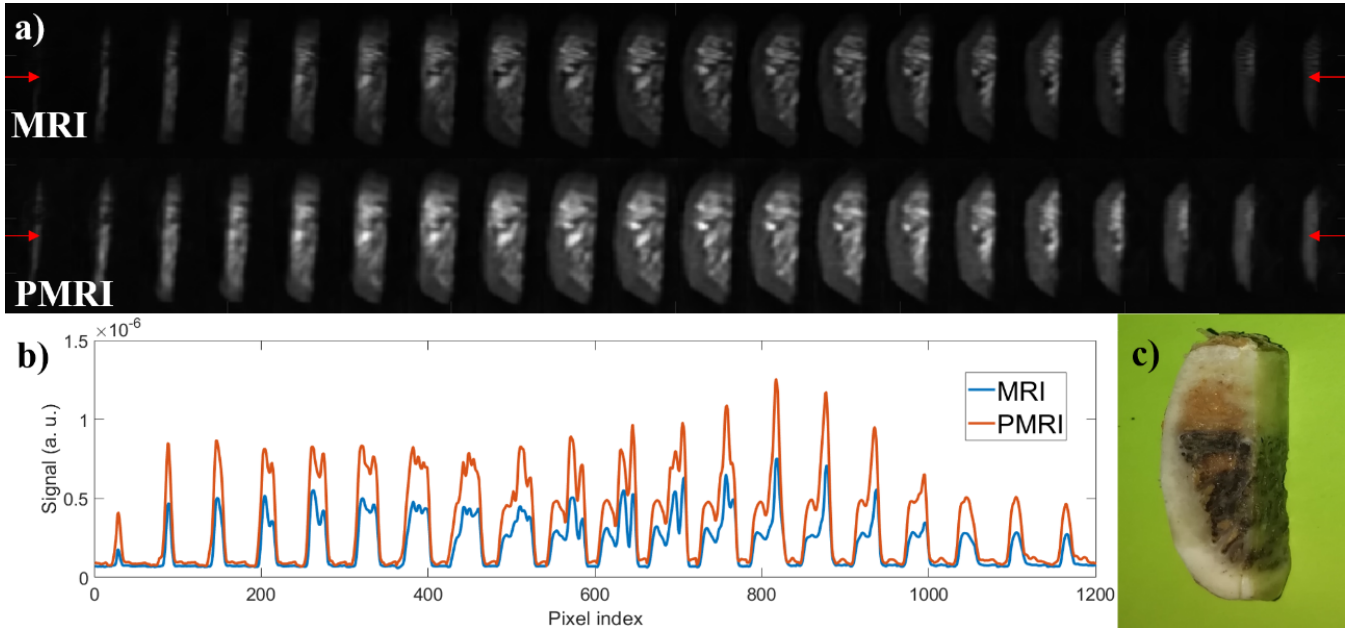


Fig. 8. (a) PETRA (top) and P-PETRA (bottom) images of an *ex-vivo* piece of cattle rib bone. (b) Signal intensity along the horizontal line defined by the red arrows in (a). The experimentally obtained value for the prepolarization SNR gain is $\alpha \approx 1.99$ (expected value ≈ 2.00 , see text). (c) Photograph of the sample.

of interest. For comparison, the expected prepolarization gain from Eq. (2) is ≈ 2.02 .

We have applied an analogous protocol to image a piece of a cattle rib bone. The size of the field of view is set to $36 \times 15 \times 15 \text{ mm}^3$ and the image is reconstructed with ART into $72 \times 30 \times 30$ voxels. The acquisition starts $t_{\text{del}2} = 125 \mu\text{s}$ after the RF pulse and lasts $t_{\text{acq}} = 800 \mu\text{s}$, with a bandwidth $BW \approx 45 \text{ kHz}$. The repetition time is $TR = 280 \text{ ms}$. The k -space undersampling is again $\times 8$. Every image contains 11 averages for a total scan time of $\approx 53 \text{ min}$. The bottom

row of images in Fig. 8(a) corresponds to scans in which a prepolarization pulse is triggered with a current intensity of $\approx 260 \text{ A}$ ($B_t \approx 0.56 \text{ T}$), which lasts $t_p = 90 \text{ ms}$ and where $t_{\text{del}1} = 1.5 \text{ ms}$. The pulse sequence for the top row of Fig. 8(a) is identical, but the prepolarization pulse is not triggered ($B_p = 0$, $B_t = 0.26 \text{ T}$). The brightness scale is again common to both datasets, and the images have been also Block-Matched filtered. The SNR enhancement is evident in Fig. 7(b), which shows the reconstructed signal intensity profile along a horizontal line around the middle region of the

images in (a). The measured mean $\alpha = \text{SNR}_{\text{PMRI}}/\text{SNR}_{\text{MRI}}$ is ≈ 1.99 , where $\text{SNR}_{\text{PMRI}} \approx 35.5$ and $\text{SNR}_{\text{MRI}} \approx 17.8$ (defined as in the previous paragraph). For comparison, the expected prepolarization gain from Eq. (2) is ≈ 2.00 .

VI. CONCLUSION AND OUTLOOK

We have shown that it is possible to enhance the quality of magnetic resonance images of hard tissues at low magnetic fields by means of a high power prepolarizer module, for a total cost of ≈ 20 k€, where the GPA 400-750 module is around 13 k€. The major challenges we have faced are: i) integrating a high power drive capable of switching off the prepolarization pulse fast enough; and ii) coping with mechanical vibrations due to the strong magnetic interaction between the main and prepolarization fields.

The preliminary results shown in this work have been obtained in a highly constrained setup in terms of prepolarizer alignment, hydraulic capacity and prepolarizer duty cycle. If the prepolarization field were aligned with the main static field, we could have approached $B_t = 0.74$ T, leading to an increase in SNR of $\times 2.85$. Also, limitations in the cooling system forced us to work under 260 A, where the system could have taken up to 320 A. This corresponds to $B_t \approx 0.66$ T with the current configuration, or $B_t \approx 0.92$ T if \vec{B}_0 and \vec{B}_p are aligned. A further limitation of our setup is the maximum duty cycle of the GPA 400-750 module, which enforces repetition times $\text{TR} \geq 250$ ms. These are significantly longer than strictly required by the T_1 values of the samples. Assuming a hypothetical $\text{TR} \geq 4T_1$, enough to thermalize at 98 % of the longitudinal magnetization, $\text{TR} = 60$ ms would have sufficed for prepolarization of teeth. Without these limitations, i.e. with $\text{TR} = 60$ ms (shorter acquisitions), $I_p = 320$ A and $\vec{B}_p \parallel \vec{B}_0$, we could achieve $B_t \approx 0.92$ T and $\alpha \approx 3.5$, compared to $B_t \approx 0.56$ T and $\alpha \approx 2$.

The results in this paper are of potential application to clinical dental MRI. This would require a prepolarizer magnet large enough to fit a human head. Matter *et al.* made a 0.4 T prepolarizer of ≈ 127 mm in diameter, which they used for *in vivo* PMRI of a human wrist [12]. We argue next that a larger coil for dental applications is also realistic. The magnetic field strength inside a solenoid of inner (outer) radius r_{in} (r_{out}) and length l is given by

$$B_p = \mu_0 G(\alpha, \beta) \sqrt{\frac{P\lambda}{\rho r_{\text{in}}}}, \quad (5)$$

where μ_0 is the vacuum permeability, P is the power dissipated in the coil due to resistive losses, λ is the fraction of conductor material in the solenoid (to account for water refrigeration conducts, isolating material and gaps between windings and layers), ρ is the resistivity of the conductor, and $G(\alpha, \beta)$ is a geometric factor defined as

$$G(\alpha, \beta) = \sqrt{\frac{\beta}{2\pi(\alpha^2 - 1)}} \left(\sinh^{-1}(\alpha/\beta) - \sinh^{-1}(1/\beta) \right), \quad (6)$$

with $\alpha = r_{\text{out}}/r_{\text{in}}$ and $\beta = l/(2r_{\text{in}})$ [12], [33]. Assuming the same copper wire as in Ref. [12] (square section of side 4 mm with a hole of radius 1 mm), a solenoid with $n_1 = 7$ layers

with $n_w = 55$ windings each would have a total resistance $R \approx 0.41 \Omega$ for $r_{\text{in}} = 115$ mm, $r_{\text{out}} = 143$ mm and $l = 220$ mm. For a drive current $I_p = 210$ A, the dissipated power is $P = RI_p^2 \approx 18$ kW and $B_p \approx 0.3$ T. For comparison, the wrist coil in Ref. [12] produces 0.4 T at 16 kW. The inductance of the prepolarizer coil can be estimated as [34]

$$L_p \approx 7.87 \mu\text{H} \times \frac{(r_{\text{out}} + r_{\text{in}})^2 n_w^2 n_1^2}{3(r_{\text{out}} + r_{\text{in}}) + 9l + 10(r_{\text{out}} - r_{\text{in}})}, \quad (7)$$

where all distances must be given in meters. Using the above numbers we find $L_p \approx 26$ mH. With the 750 V available from the GPA 400-750 unit, the current could be switched off in a time $t_{\text{off}} \approx 7$ ms, still significantly shorter than the T_1 of the hardest human tissues. At these field variation rates (50 T/s), unwanted magneto-stimulation effects may take place [35]. This can be further investigated in dedicated setups [36] and, if required, the prepolarization coil could be designed specifically to avoid peripheral nerve stimulation [37], [38].

CONTRIBUTIONS

The high power electronics for prepolarization were designed and installed by JMG, JB, JPR and JA. The prepolarizer and mechanical holder were designed, assembled and characterized by JPR, JMG, EP and JB, with contributions from DGR and JA. Experimental data in the ‘‘DentMRI - Gen I’’ scanner were taken by JB and JMG, with help from JMA, FG, RP and JA. Data analysis performed by JB and JMG, with input from JMA, FG, RP and JA. Animal handling and manipulation of biological tissues performed by JB. The paper was written by JB, FG and JA, with input from all authors. Experiments conceived by JMB, JA and AR.

ACKNOWLEDGMENT

This work was supported by the Ministerio de Ciencia e Innovaci3n of Spain through research grant PID2019-111436RB-C21. Action co-financed by the European Union through the Programa Operativo del Fondo Europeo de Desarrollo Regional (FEDER) of the Comunitat Valenciana 2014-2020 (IDIFEDER/2018/022). JMG and JB acknowledge support from the Innodocto program of the Agencia Valenciana de la Innovaci3n (INNTA3/2020/22 and INNTA3/2021/17).

ETHICAL STATEMENT

All animal parts were obtained from a local butcher and research was conducted following the 3R principles. Experiments using human teeth were approved by the medical center Cl3nica Llobell Cortell S.L. Procedures were conducted following the approved protocols, and informed consent was obtained from participants prior to study commencement.

REFERENCES

- [1] M. Sarracanie, C. D. LaPierre, N. Salameh, D. E. J. Waddington, T. Witzel, and M. S. Rosen, ‘‘Low-Cost High-Performance MRI,’’ *Scientific Reports*, vol. 5, no. 1, p. 15177, dec 2015. [Online]. Available: <http://www.nature.com/articles/srep15177>
- [2] J. P. Marques, F. F. Simonis, and A. G. Webb, ‘‘Low-field MRI: An MR physics perspective,’’ *Journal of Magnetic Resonance Imaging*, vol. 49, no. 6, pp. 1528–1542, jun 2019. [Online]. Available: <https://onlinelibrary.wiley.com/doi/abs/10.1002/jmri.26637>

- [3] M. Sarracanie and N. Salameh, "Low-Field MRI: How Low Can We Go? A Fresh View on an Old Debate," *Frontiers in Physics*, vol. 8, p. 172, jun 2020. [Online]. Available: <https://www.frontiersin.org/article/10.3389/fphy.2020.00172/full>
- [4] A. Macovski and S. Conolly, "Novel approaches to low-cost MRI," *Magnetic Resonance in Medicine*, vol. 30, no. 2, pp. 221–230, 1993.
- [5] P. Morgan, S. Conolly, G. Scott, and A. Macovski, "A readout magnet for prepolarized MRI," *Magnetic Resonance in Medicine*, vol. 36, no. 4, pp. 527–536, oct 1996. [Online]. Available: <http://doi.wiley.com/10.1002/mrm.1910360405>
- [6] C. Kessler, H. Seton, and J. Hutchison, "Prepolarized fast spin-echo pulse sequence for low-field MRI," *Magnetic Resonance in Medicine*, vol. 57, no. 6, pp. 1180–1184, jun 2007. [Online]. Available: <http://doi.wiley.com/10.1002/mrm.21238>
- [7] S. K. Lee, M. Moessler, W. Myers, N. Kelso, A. H. Trabesinger, A. Pines, and J. Clarke, "SQUID-detected MRI at 132 uT with T1-weighted contrast established at 10 uT–300 mT," *Magnetic Resonance in Medicine*, vol. 53, no. 1, pp. 9–14, jan 2005. [Online]. Available: <http://doi.wiley.com/10.1002/mrm.20316>
- [8] J. Obungoloch, J. R. Harper, S. Consevage, I. M. Savukov, T. Neuberger, S. Tadigadapa, and S. J. Schiff, "Design of a sustainable prepolarizing magnetic resonance imaging system for infant hydrocephalus," *Magnetic Resonance Materials in Physics, Biology and Medicine*, vol. 31, no. 5, pp. 665–676, oct 2018. [Online]. Available: <https://doi.org/10.1007/s10334-018-0683-y>
- [9] J. M. Algarín, E. Díaz-Caballero, J. Borreguero, F. Galve, D. Grau-Ruiz, J. P. Rigla, R. Bosch, J. M. González, E. Pallás, M. Corberán, C. Gramage, S. Aja-Fernández, A. Ríos, J. M. Benlloch, and J. Alonso, "Simultaneous imaging of hard and soft biological tissues in a low-field dental MRI scanner," *Scientific Reports*, vol. 10, no. 1, p. 21470, 2020. [Online]. Available: <https://doi.org/10.1038/s41598-020-78456-2>
- [10] J. P. Rigla, J. Borreguero, C. Gramage, E. Pallas, J. M. Gonzalez, R. Bosch, J. M. Algarin, J. V. Sanchez-Andres, F. Galve, D. Grau-Ruiz, R. Pellicer, A. Rios, J. M. Benlloch, and J. Alonso, "A Fast 0.5 T Prepolarizer Module for Preclinical Magnetic Resonance Imaging," *IEEE Transactions on Magnetics*, 2021.
- [11] J. Kowalewski and L. Mäler, *Nuclear spin relaxation in liquids: theory, experiments, and applications*. Taylor & Francis, 2006.
- [12] N. Matter, G. Scott, T. Grafendorfer, A. Macovski, and S. Conolly, "Rapid polarizing field cycling in magnetic resonance imaging," *IEEE Transactions on Medical Imaging*, vol. 25, no. 1, pp. 84–93, jan 2006. [Online]. Available: <http://ieeexplore.ieee.org/document/1564329/>
- [13] N. I. Matter, G. C. Scott, R. D. Venook, S. E. Ungersma, T. Grafendorfer, A. Macovski, and S. M. Conolly, "Three-Dimensional Prepolarized Magnetic Resonance Imaging Using Rapid Acquisition with Relaxation Enhancement," *Magnetic Resonance in Medicine*, vol. 56, pp. 1085–1095, 2006. [Online]. Available: www.interscience.wiley.com]
- [14] R. D. Venook, N. I. Matter, M. Ramachandran, S. E. Ungersma, G. E. Gold, N. J. Giori, A. Macovski, G. C. Scott, and S. M. Conolly, "Prepolarized magnetic resonance imaging around metal orthopedic implants," *Magnetic Resonance in Medicine*, vol. 56, no. 1, pp. 177–186, jul 2006. [Online]. Available: <http://doi.wiley.com/10.1002/mrm.20927>
- [15] I. Savukov and T. Karaulanov, "Magnetic-resonance imaging of the human brain with an atomic magnetometer," *Applied Physics Letters*, vol. 103, no. 4, p. 043703, jul 2013. [Online]. Available: <http://aip.scitation.org/doi/10.1063/1.4816433>
- [16] B. Inglis, K. Buckenmaier, P. Sangiorgio, A. F. Pedersen, M. A. Nichols, and J. Clarke, "MRI of the human brain at 130 microtesla." *Proceedings of the National Academy of Sciences of the United States of America*, vol. 110, no. 48, pp. 19194–201, nov 2013. [Online]. Available: <http://www.ncbi.nlm.nih.gov/pubmed/2425511> <http://www.pubmedcentral.nih.gov/articlerender.fcgi?artid=PMC3845112>
- [17] M. J. Duer, *Introduction to solid-state NMR spectroscopy*. Blackwell Oxford, 2004.
- [18] N. Shah, "Recent advances in imaging technologies in dentistry," *World Journal of Radiology*, vol. 6, no. 10, p. 794, 2014.
- [19] S. Mastrogiacomo, W. Dou, J. A. Jansen, and X. F. Walboomers, "Magnetic Resonance Imaging of Hard Tissues and Hard Tissue Engineered Bio-substitutes," *Molecular Imaging and Biology*, vol. 21, no. 6, pp. 1003–1019, dec 2019. [Online]. Available: <http://link.springer.com/10.1007/s11307-019-01345-2>
- [20] D. Idiyatullin, C. Corum, S. Moeller, H. S. Prasad, M. Garwood, and D. R. Nixdorf, "Dental magnetic resonance imaging: making the invisible visible," *Journal of endodontics*, vol. 37, no. 6, pp. 745–752, 2011.
- [21] M. Weiger, K. P. Pruessmann, A.-K. Bracher, S. Köhler, V. Lehmann, U. Wolfram, F. Hennel, and V. Rasche, "High-resolution ZTE imaging of human teeth," *NMR in Biomedicine*, vol. 25, no. 10, pp. 1144–1151, oct 2012. [Online]. Available: <http://doi.wiley.com/10.1002/nbm.2783>
- [22] R. Rai, D. Manton, M. Jameson, S. Josan, M. Barton, L. Holloway, and G. Liney, "3d printed phantoms mimicking cortical bone for the assessment of ultrashort echo time magnetic resonance imaging," *Medical Physics*, vol. 45, 12 2017.
- [23] G. M. Bydder, J. V. Hajnal, and I. R. Young, "MRI: Use of the inversion recovery pulse sequence," *Clinical Radiology*, vol. 53, no. 3, pp. 159–176, mar 1998.
- [24] H. Y. Carr and E. M. Purcell, "Effects of diffusion on free precession in nuclear magnetic resonance experiments," *Physical Review*, vol. 94, no. 3, pp. 630–638, 1954.
- [25] S. Meiboom and D. Gill, "Modified spin-echo method for measuring nuclear relaxation times," *Review of Scientific Instruments*, vol. 29, no. 8, pp. 688–691, 1958.
- [26] M. Weiger, D. O. Brunner, B. E. Dietrich, C. F. Müller, and K. P. Pruessmann, "Zte imaging in humans," *Magnetic Resonance in Medicine*, vol. 70, no. 2, pp. 328–332, 2013. [Online]. Available: <https://onlinelibrary.wiley.com/doi/abs/10.1002/mrm.24816>
- [27] N. Kobayashi, U. Goerke, L. Wang, J. Ellermann, G. J. Metzger, and M. Garwood, "Gradient-modulated petra mri," *Tomography*, vol. 1, no. 2, pp. 85–90, 2015. [Online]. Available: <https://www.mdpi.com/2379-139X/1/2/85>
- [28] M. Weiger and K. P. Pruessmann, "Short-t2 mri: Principles and recent advances," *Progress in Nuclear Magnetic Resonance Spectroscopy*, vol. 114–115, pp. 237–270, 2019. [Online]. Available: <https://www.sciencedirect.com/science/article/pii/S0079656519300330>
- [29] D. M. Grodzki, P. M. Jakob, and B. Heismann, "Ultrashort echo time imaging using pointwise encoding time reduction with radial acquisition (PETRA)," *Magnetic Resonance in Medicine*, vol. 67, no. 2, pp. 510–518, feb 2012.
- [30] S. Karczmarz, "Angenäherte auflösung von systemen linearer gleichungen," *Bull. Int. Acad. Pol. Sic. Let., Cl. Sci. Math. Nat.*, pp. 355–357, 1937. [Online]. Available: <https://ci.nii.ac.jp/naid/10009398882/en/>
- [31] R. M. Gower and P. Richtarik, "Randomized iterative methods for linear systems," *SIAM Journal on Matrix Analysis and Applications*, vol. 36, no. 4, pp. 1660–1690, 2015.
- [32] M. Maggioni, V. Katkovnik, K. Egiazarian, and A. Foi, "Nonlocal transform-domain filter for volumetric data denoising and reconstruction," *IEEE Transactions on Image Processing*, vol. 22, no. 1, pp. 119–133, 2013.
- [33] D. B. Montgomery, *Solenoid magnet design. The magnetic and mechanical aspects of resistive and superconducting systems*. John Wiley and Sons, Inc., New York, 1969.
- [34] American Radio Relay League., *The ARRL handbook for radio amateurs, 2000*. Newington, CT: American Radio Relay League, 1999.
- [35] International Electrotechnical Commission, "Medical electrical equipment-Part 2-33: Particular requirements for the basic safety and essential performance of magnetic resonance equipment for medical diagnosis," *IEC 60601-2-33 Ed. 3.0*, 2010.
- [36] D. Grau-Ruiz, J. P. Rigla, E. Pallás, J. M. Algarín, J. Borreguero, R. Bosch, G. Comazzi, E. Díaz-Caballero, F. Galve, C. Gramage, J. M. González, R. Pellicer, A. Ríos, J. M. Benlloch, and J. Alonso, "Peripheral Nerve Stimulation limits with fast narrow and broad-band pulses," *arXiv*, dec 2020. [Online]. Available: <http://arxiv.org/abs/2012.06232>
- [37] M. Davids, B. Guérin, M. Malzacher, L. R. Schad, and L. L. Wald, "Predicting Magnetostimulation Thresholds in the Peripheral Nervous System using Realistic Body Models," *Scientific Reports*, vol. 7, no. 1, pp. 1–14, dec 2017.
- [38] M. Davids, B. Guérin, L. R. Schad, and L. L. Wald, "Peripheral nerve stimulation modeling for MRI," *eMagRes*, vol. 8, no. 2, pp. 87–102, 2019. [Online]. Available: <https://onlinelibrary.wiley.com/doi/full/10.1002/9780470034590.emrstm1586>